Acta Biomaterialia 59 (2017) 94–107

Contents lists available at ScienceDirect

Acta Biomaterialia

journal homepage: www.elsevier.com/locate/actabiomat

Full length article

Enhanced human bone marrow mesenchymal stromal cell adhesion on scaffolds promotes cell survival and bone formation

Miryam Mebarki [a,b,c], Laura Coquelin [a,b,c], Pierre Layrolle [e], Séverine Battaglia [e], Marine Tossou [a,b,c], Philippe Hernigou [a,b,d], Hélène Rouard [a,b,c], Nathalie Chevallier [a,b,c,*]

[a] IMRB U955-E10, INSERM, Creteil, France
[b] Faculty of Medicine, Paris Est University, Creteil, France
[c] Engineering and Cellular Therapy Unit, Etablissement Français du Sang, Créteil, France
[d] Orthopaedic Surgery Department, Henri-Mondor AP-HP Hospital, Creteil, France
[e] INSERM U957, Lab. Pathophysiology of Bone Resorption, Faculty of Medicine, University of Nantes, Nantes, France

ARTICLE INFO

Article history:
Received 9 February 2017
Received in revised form 8 June 2017
Accepted 13 June 2017
Available online 19 June 2017

Keywords:
Mesenchymal stem cells
Biomaterial
Cell therapy
Bone tissue engineering
HA/βTCP
Tutoplast

ABSTRACT

In order to induce an efficient bone formation with human bone marrow mesenchymal stromal cells (hBMSC) associated to a scaffold, it is crucial to determine the key points of the hBMSC action after *in vivo* transplantation as well as the appropriate features of a scaffold. To this aim we compared the hBMSC behavior when grafted onto two biomaterials allowing different bone potential *in vivo*. The cancellous devitalized Tutoplast®-processed bone (TPB) and the synthetic hydroxyapatite/β-tricalcium-phosphate (HA/βTCP) which give at 6 weeks 100% and 50% of bone formation respectively. We first showed that hBMSC adhesion is two times favored on TPB *in vitro* and *in vivo* compared to HA/βTCP. Biomaterial structure analysis indicated that the better cell adhesion on TPB is associated to its higher and smooth open pore architecture as well as its content in collagen. Our 6 week time course analysis, showed using qPCR that only adherent cells are able to survive *in vivo* giving thus an advantage in term of cell number on TPB during the first 4 weeks after graft. We then showed that grafted hBMSC survival is crucial as cells participate directly to bone formation and play a paracrine action via the secretion of hIGF1 and hRANKL which are known to regulate the bone formation and resorption pathways respectively. Altogether our results point out the importance of developing a smooth and open pore scaffold to optimize hBMSC adhesion and ensure cell survival *in vivo* as it is a prerequisite to potentiate their direct and paracrine functions.

Statement of Significance

Around 10% of skeletal fractures do not heal correctly causing nonunion. An approach involving mesenchymal stromal cells (MSC) associated with biomaterials emerges as an innovative strategy for bone repair. The diversity of scaffolds is a source of heterogeneity for bone formation efficiency. In order to better determine the characteristics of a powerful scaffold it is crucial to understand their relationship with cells after graft. Our results highlight that a biomaterial architecture similar to cancellous bone is important to promote MSC adhesion and ensure cell survival *in vivo*. Additionally, we demonstrated that the grafted MSC play a direct role coupled to a paracrine effect to enhance bone formation and that both of those roles are governed by the used scaffold.
© 2017 Acta Materialia Inc. Published by Elsevier Ltd. This is an open access article under the CC BY-NC-ND license (http://creativecommons.org/licenses/by-nc-nd/4.0/).

1. Introduction

Bone has the particularity to regenerate after a lesion allowing fracture repair in 6–8 weeks [1]. Bone regeneration is mostly spontaneous and surgery occurs only to mechanically stabilize the fracture [2]. However, 5 to 10% of skeletal fractures do not heal correctly causing delayed union or nonunion called pseudarthrosis

* Corresponding author at: Etablissement Français du Sang d'Ile-de-France, Unité d'Ingénierie et de Thérapie Cellulaire, 5 rue Gustave Eiffel, 94017 Créteil cedex, France.
E-mail address: nathalie.chevallier@efs.sante.fr (N. Chevallier).

http://dx.doi.org/10.1016/j.actbio.2017.06.018
1742-7061/© 2017 Acta Materialia Inc. Published by Elsevier Ltd.
This is an open access article under the CC BY-NC-ND license (http://creativecommons.org/licenses/by-nc-nd/4.0/).

[3]. These defects require additional interventions with a major impact on patient life quality and with socio-economic burden [2,3]. To manage this problem, different therapeutic strategies have been developed. Autologous cancellous bone graft is still until today the gold standard for regeneration of bone defects exceeding 4 cm [2]. Although this bone transplantation approach has shown its clinical efficacy, it presents several drawbacks (i.e. limited bone stock, additional surgical site with consequent pain and risk of infections) [4]. Other approaches have been developed for clinical use. Allogeneic bone graft (i.e. surgical waste, post-mortem donors) is an alternative to autograft [5]. Bone xenograft has also been used, such as bovine bone whose structure is close to humans [6]. However, these strategies may transfer pathogens [7] or lead to immunological reactions [8]. To overcome bone graft disadvantages, several biocompatible scaffolds have been developed [9–11]. Synthetic bioceramics of hydroxyapatite (HA); tricalcium phosphate (TCP) or their mixture biphasic calcium phosphate (BCP) are the most used in skeletal engineering because of their osteoconductive properties and the easy management of their architecture [12]. Alternative natural scaffolds including secure amorphous human bone [9,10], animal derived bone matrices [13] or the coral exoskeleton [11] offer a similar structure to cancellous bone and thus mimic the physiological bone tissue environment [12]. However, when used alone these scaffolds lack osteoinductive properties and serve only to guide bone tissue [4]. To enhance new bone formation, growth factors (FGF-2, PDGFs) or differentiating factors (BMPs) and more recently stem cells have been associated to these scaffolds [3,14,15]. An approach involving human bone marrow mesenchymal stromal cells (hBMSC) associated with biomaterials emerges as an innovative strategy to repair delayed unions [11]. Mesenchymal stromal cells (MSC) ability to differentiate into several tissues including bone, cartilage and adipose [16] was widely exploited for tissue regeneration. While their capacity to induce bone formation has been proven, mechanisms of fracture repair remain controversial. Several studies suggest a direct contribution of MSC to regenerate bone as they differentiate into osteoblastic lineage when implanted locally or even when administrated systemically [17,18,23]. Ponte et al., suggest that the host inflammatory environment at the injury site induces the recruitment and the engraftment of MSC [19]. This homing can be under the control of SDF-1/CXCR-4 signaling [20,21] but also mediated by other cytokines such as IGF-1 and PDGF [19]. Nonetheless, divergent studies are in favor of a paracrine effect of grafted MSC on host cells *via* the release of cytokines and growth factors. In response to inflammation at the bone lesion site, grafted MSC secrete immunomodulatory cytokines such as prostaglandin 2, TGF-β1, TNF-α, IL-4, 6 and 10 to prevent proliferation of inflammatory cells including T and B lymphocytes, natural killer cells and macrophages [22,23]. In addition, secretion of factors such as SDF-1 and macrophage inflammatory protein-1 α and β reduce scar tissue formation [22]. MSC are also able to initiate angiogenesis and enhance endothelial cells recruitment and proliferation through secreted growth factors including VEGF, IGF-1, angiopoietin-1 and EGF [24]. It has also been shown that hBMSC recruit macrophages and osteoclasts at the site of implantation prior to bone formation [25]. In summary, MSC ability to differentiate in bone lineage, associated to their paracrine functions and their availability, make them a promising candidate in regenerative medicine [22]. Hence, these properties were clinically exploited to develop a minimally invasive therapeutic strategy for bone repair [26–28].

Our team demonstrated that hBMSC expansion e*x vivo* using human platelet lysate accelerates their proliferation and prime their osteogenic differentiation [29]. This strategy allows the use of a growth factors cocktail (e.g. BMPs, TGF-b1, IGF, bFGF, PDGF, PF-4, interleukin-1, and osteonectin) to stimulate multiple signaling pathways, as opposed to previous strategies where a single recombinant growth factor was used and acted only on one molecular pathway [29,30]. Moreover, we and other observed a variability in the osteoconductive and osteoinductive properties of different bone allografts or ceramics resulted in differences in *in vivo* bone formation [10,31]. Cell attachment and metabolism vary between scaffolds having the same composition but with different structures [31,32] demonstrating that the scaffold geometry is crucial to guide bone formation [33].

In order to induce an efficient bone formation, it is crucial to determine the key points of the hBMSC action after graft *in vivo* as well as to determine the main characteristic of a powerful scaffold. To this aim we followed and compared during a 6 week time course, the *in vivo* hBMSC behavior when grafted onto two different biomaterials allowing different bone potential. To this end, the cancellous devitalized Tutoplast®-processed bone (TPB) and the synthetic hydroxyapatite/β-tricalcium-phosphate (HA/βTCP) which are clinically used as bone substitutes [9,29,31,34]. Human BMSC were collected from several donors, amplified *in vitro* and then loaded extemporaneously on scaffolds implanted subcutaneously in SCID mice, as this model is more efficient to induce *in vivo* bone formation [34]. After having evaluated the biomaterial impact on ectopic bone formation, we evaluated during a 6 week time course, their impact on cell attachment and survival, on cell dissemination as well as on hBMSC behavior and function. We then performed *in vitro* analysis in order to discriminate the direct relationship between the scaffold structure and the *in vivo* cell feature.

2. Materials and methods

2.1. Biomaterials

Two scaffolds with different structure and composition were used. (1) Hydroxyapatite (65%)/beta-tricalcium phosphate (35%) (HA/βTCP) (Ceraver, France) is composed of 60 ± 5% macropores (100 to 400 μm pore diameter) and 40 ± 5% micropores (<10 μm pore diameter). (2) Tutoplast®-processed human bone (TPB) (EFS, Ile de France). The bone Tutoplast®-process (Tutogen Medical) consists in a delipidization, an osmotic cell destruction treatment, hydrogen peroxide treatment, and washing cycles for the removal of the noncollagen proteins followed by a solvent dehydrated step and finally a γ-irradiation procedure. Both biomaterials were in the form of irregular granules sizing 2–3 mm and weighing 8.0 ± 1 mg.

2.2. Physico-chemical characterization of biomaterials

The microstructure of the scaffolds was investigated by using a scanning electron microscope (SEM; Hitachi TM3000 Tabletop Microscope, Tokyo, Japan). Prior to SEM observations, the samples were coated with a thin film of carbon obtained by glow discharge (Leica, ACE 200, Germany). Powder X-ray diffraction (XRD, Siemens D5000 Moxtek) was performed on crushed scaffolds to determine the phases and crystallinity using the monochromatic source KαCu. Fourier Transform Infrared Spectroscopy (FTIR, Bruker, Vertex 70) was performed on KBr pellets with 1 mg of sample mixed with 300 mg of KBr and pressed at 5 tons. Micro-computed tomography (μCT, Skyscan 1076 *in vivo* model, Kontich, Belgium) of scaffolds was performed. Briefly, the X-ray source was operated at 50 kV and acquisitions were recorded around 180° with step angle of 0.7°. Three dimensional (3D) reconstructions were performed using the Skyscan software CTRecon. The morphometric parameters, Percent Object Volume/Total Volume (Obj.V/TV, %), Object Surface (Obj.S, mm^2) and Open Porosity (%) of both scaffolds were measured by using the Skyscan™ CT-ANalyzer software (n = 5 samples/biomaterial scaffold).

2.3. Ethical statements

Bone marrow (BM) was collected from the iliac crest of 5 anonymized patients after having received their informed consent under the ethical committee approval N° DC.-2009-1049. All animal experimental protocols were approved by the local ethical committee Anses/ENVA/UPEC N°18/11/14-1.

2.4. Preparation of human platelet lysate (PL)

PL was obtained from platelet apheresis collections performed at the "Etablissement Français du Sang" (Rungis, France). All apheresis products were biologically qualified according to French legislation. The platelet count in each product was measured automatically (ABX penta 60 C+, Horiba ABX, France). For homogenizing PL preparation, 6–10 human blood samples were mixed to adjust the concentration at $3 \pm 0.5 \times 109$ platelets/ml, frozen at −80 °C and subsequently used to obtain PL containing platelet-released growth factors. Remaining platelet bodies were eliminated by centrifugation (1400*g*). All PL batches were qualified for their cell growth potential and three of them were used in this study.

2.5. Human bone marrow derived stromal cells (hBMSC) cultures

Human BMSC were isolated from BM as previously described [29]. In this project, hBMSC were thawed between passage 1 and 3, seeded at 2×103 cells/cm^2 for expansion and then used at passage 2 or 3 for *in vivo* experiment and at passage 3 or 4 for *in vitro* experiment. Culture medium contained α-modified Eagle's medium (αMEM) (ThermoFisher, France) supplemented with 5% human platelet lysate (PL), 0.5% Ciprofloxacine (Bayer Pharma, France) and 2 IU/ml Heparin (Sanofi-Aventis, France) to avoid clot formation. Cultures were maintained in a humidified atmosphere with 5% CO_2 at 37 °C and the culture medium changed twice a week. When reaching confluence, cells were detached using trypsin/EDTA (Life technologies). Time of doubling (TD) were determined after cell passage. TD was calculated using the equation $(T \times \log 2)/(\log Y - \log X)$ (where X is the number of cells originally plated, Y the number of cells at confluence and T the time of culture in hours) [35]. TD were equivalent for the three BM donors used *in vivo* and *in vitro* (TD = 37.7 ± 8.6 for donor 1; TD = 34.9 ± 2.0, donor 2; TD = 36.5 ± 5.9, donor 3). As for the 2 other BM donors used for the *in vitro* gene expression analysis (TD = 34.7 ± 1.6, donor 4; TD = 39.3 ± 2.3, donor 5).

2.6. Animal surgery

A minimum of six SCID male mice of 7 week-old were used per time point (Charles River laboratories, France). Under general anesthesia by Isoflurane (Abbott, France) and after shaving off dorsal hair, skin incisions of 5 mm were made. Six subcutaneous pockets of 4–5 mm in depth were prepared on each mouse. The granule of HA/βTCP or TPB scaffold of 2–3 mm weighing 8.0 ± 1 mg was inserted in the subcutis pocket and 10^6 hBMSC were extemporaneously loaded on each biomaterial granule as previously described [34]. Incisions were immediately sutured with 5–0 sutures (Ethicon, USA). Animals were sacrificed by an overdose of pentobarbital (120 mg/kg, Ceva Santé Animale, France) at 24, 48 and 72 h (h) then, at 1, 2, 4 and 6 weeks (W) after implantation. The samples were dissected and harvested for histology or for molecular biology analysis. Adjacent tissues and organs were collected in conjunction. Cell-free biomaterial scaffolds served as controls.

2.7. Histological analysis

Samples were immediately fixed in 4% paraformaldehyde (Millipore, Germany) for 4 h at room temperature then in 70% ethanol (Cooper, France) overnight at 4 °C. After fixation, samples were decalcified in 19% EDTA (Sigma-Aldrich, Germany) at 50 °C for 24–72 h using an automate (KOS Microwave HistoStation, Milestone Medical, USA). All the samples were dehydrated in graded ethanol baths and embedded in paraffin. Sections of 3 μm in thickness were made using a microtome (Microm HM 355S, ThermoFisher Scientific, USA) and stained with Masson's trichrome. This staining combines hematein for cell nuclei (purple/black), fuschsin Ponceau for cytoplasm, muscle and erythrocytes (red) and light green solution for collagen (green/blue). Six samples per time point and 8–12 sections selected throughout 800 μm of each sample were analyzed. The images were acquired with a standard light microscope (Olympus, CX41, Japan) using a Digital Colour Camera (UC30) and CellSens Entry software (Olympus, Japan). The frequency of bone formation was estimated as the number of scaffolds with newly formed bone related to the total number of implanted scaffolds. Only scaffolds supporting bone formation were then analyzed. The quantity of new bone and bone marrow (BM) was measured using ImageJ software (National Institutes of Health, USA) and expressed as the percentage of newly formed bone and BM area related to the total implant area.

2.8. In situ apoptosis detection

Apoptosis was evaluated using TACS® 2 TdT DAB In Situ Apoptosis Detection Kit (Trevigen®, USA) at 24 h, 48 h and 72 h post-graft, on biomaterials associated with hBMSC (n = 3 samples/time point and n = 3 sections/sample). Briefly, TdT nucleotides are incorporated in fragmented DNA of apoptotic cells then detected by the complex Biotin/Streptavidin/Label. Samples were prepared similarly to histological analysis and apoptotic cells were stained following manufacturer protocol. The images were acquired with a standard light microscope (Olympus CX41, Japan) using Digital Colour Camera (UC30) and CellSens Entry software (Olympus, Japan). Mouse scar skin harvested 24 h after injury was used as a positive control of apoptotic cells.

2.9. Immunostaining analysis

To detect grafted human BMSC in host mice, immunohistochemistry of human lamin AC was performed 24 h post-graft using a mouse anti-human lamin AC antibody (NCL-LAM-A/C, Novocastra laboratories, UK) followed by a goat anti-mouse IgG poly-HRP secondary antibody (AP340P, Merck Millipore, France) and peroxidase was detected using DAB substrate (Vector Laboratories). Sections were counterstained with hematoxylin, mounted in Eukitt and examined by a standard light microscope (Olympus CX41, France). Cell-free biomaterials were used as negative controls.

Immunofluorescence detection of human bone sialoprotein (hIBSP) was performed using a rabbit anti-hIBSP primary antibody (ab52128, Abcam, UK) and a biotinylated goat anti-rabbit secondary antibody (BA-1000, Vector Laboratories), then revealed with streptavidin Alexa Fluor® 647 conjugate (Life Technologies, France). Mouse femoral bone have been used to validate the hIBSP antibody specificity. No cross reactivity have been found (data not shown). Nuclei were stained with 4′,6′-diamidino-2-phenylindole (DAPI) (Sigma) and sections were mounted in Fluoromount G (eBioscience, France). Fluorescence was analyzed with a fluorescence microscope (AxioImager D1, Zeiss) in sequential scanning mode for triple detection: Alexa 647 for hIBSP detection, DAPI for nucleus detection and green autofluorescence for scaffold and bone extracellular matrix detection. Quantification of hIBSP positive

areas was performed on 2–3 sections in each implant (n = 2 implant/donor, n = 3 donors) using ImageJ software. Results were expressed as the percentage of hIBSP$^+$ staining area related to the total neoformed bone area. Negative controls were performed on mouse femur sections and no labelling was detected, confirming the human specificity of the observed staining.

2.10. Analysis of hBMSC attachment on scaffolds with scanning electron microscopy (SEM)

Three hours post-seeding of 3 × 105 hBMSC per biomaterial, samples were fixed with 2.5% glutaraldehyde (Sigma-Aldrich, France) at 4 °C overnight, and then dehydrated with increasing concentrations of ethanol (70–100%). The dehydration was completed with 60 min of incubation with hexamethyldisilazane (Sigma-Aldrich, France). Scaffolds were then air-dried, sputtered with nano-gold film, and analyzed with scanning electron microscope (JEOL JSN-6301F) at LISA laboratories (Paris Est University, France).

2.11. Quantitative real time polymerase chain reaction (qPCR)

Biomaterials, biomaterial adjacent tissues (skin and muscle) and organs (heart, kidney, spleen, liver and lung) were cut into small pieces and weighed (up to 10 mg for spleen and up to 25 mg for other tissues), before being placed in DNA lysis buffer (Qiagen, France) and ground using the FastPrep-24® tissue and cell homogenizer (MP Biomedicals). Total DNA was isolated using QIAamp® DNA Investigator Kit as described by the manufacturer (Qiagen, France). Human DNA was quantified as previously described [34,36] using human TaqMan® Copy Number Reference Assay, RNase P (Applied Biosystems, France), and monitored with a 7500HT Fast Real-Time PCR System (Applied Biosystems). Results were normalized to that of time T0 ($\Delta Ct = Ct_{time\ Tx} - Ct_{time\ T0}$) and were reported to the total amount of DNA obtained for each implant. Results were expressed as the number of grafted hBMSC per scaffold. Quantification for each donor (n = 3 donors) was performed on n = 4 implants/donor at 24 h, 1 W and 4 W and on n = 2 implants/donor at 48 h, 2 W and 6 W.

2.12. Quantitative real time reverse transcription polymerase chain reaction (RT-qPCR)

Collected samples were immediately placed in TRIzol® reagent (Invitrogen) and biomaterials were ground using the FastPrep-24® tissue and cell homogenizer (MP Biomedicals). Total RNA was isolated using the TRIzol® reagent method as described by the manufacturer, DNAse-treated (ThermoFisher Scientific, USA) and reverse transcribed using Superscript III Reverse transcriptase (Invitrogen). Q-PCR was performed using Power SYBR®Green PCR Master Mix (Roche) and the rate of dye incorporation was monitored using the 7500HT Fast Real-Time PCR System (Applied Biosystems). The primers (Table 1) were designed and controlled for no cross-reaction between species and an efficiency of 100 ± 10% was obtained for each standard curves. Two biological replicates were used for each condition. GAPDH transcript levels were used for normalization of each target (ΔCt) and results were reported as relative gene expression ($2^{-\Delta Ct}$).

2.13. Quantification of hBMSC in vitro

After 3 h of incubation with 10^6 hBMSC on each biomaterial granule, samples were removed and ground using the FastPrep-24® tissue and cell homogenizer (MP Biomedicals) then total DNA was isolated using QIAamp® DNA Investigator Kit as described by the manufacturer (Qiagen, France). Remaining cells at the bottom of the wells were lysed in Tris–EDTA (TE) + 0.1% Triton X-100 and digested with 0.2 mg/ml proteinase K solution (Invitrogen) for 12 h at 52 °C. Then the suspension was subjected to a succession of three heat shocks, followed by sonication of the lysates for 10 min. At the same time a standard cell range from 0 to 10^6 cells was prepared. DNA samples from scaffolds, non-adherent cells and cell standard range were labelled with Picogreen solution of Quant-it Picogreen kit (Invitrogen Life Technologies, France) which only binds double-stranded DNA. After 10 min of incubation in the dark, the fluorescence was read at 520 nm using a Victor X3 Multilabel Plate Reader (PerkinElmer, France). Triplicate analysis was performed for each donor (n = 3 donors). The standard curve was then used to quantify the cells.

2.14. Quantification of in vivo osteoclastic resorption activity

Tartrate-resistant acid phosphatase (TRAP) activity was evaluated using acid phosphatase leucocyte kit (Sigma-Aldrich, USA). Paraffin sections were deparaffinised, rehydrated through alcohol gradient before being incubated in TRAP buffer (glacial acetic acid 0.02% + acetate solution 0.04% + tartrate solution 0.02% + Formamid 0.001%) and TRAP staining (Fast Garnet GBC base solution 0.011% + sodium nitrite solution 0.011% + naphtol AS-BI phosphoric acid solution 0.01%) mix for 1h30 at 37 °C, washed twice with demineralized water and mounted with Eukitt® mounting medium. Microscopic images were captured using a UC30 Digital Colour Camera and CellSens Entry software (Olympus, Japan). TRAP positive cell number and their contact area with scaffold were quantified throughout 800 μm of each sample (n = 6 samples/time point and n = 5 sections/sample) using ImageJ software.

2.15. Statistical analysis

Statistical analysis was performed using GraphPad Prism5 software using appropriate tests as specifically indicated in each figure. All values are expressed as mean ± standard error of the mean (SEM) (unless specified) and a minimum of 95% confidence interval was established for significance. For kinetic analysis, data were considered independent as different animals were grafted, then sacrificed at each time point. A p-value < 0.05 was considered statistically significant.

3. Results

3.1. Biomaterials impact bone neoformation and maturation

To evaluate the impact of biomaterials on hBMSC inducing bone formation a time course analysis was performed. Human BMSC were implanted subcutaneously on HA/βTCP or TPB scaffolds in SCID mice model and bone and bone marrow neoformation were evaluated at 2, 4 and 6 weeks (W) post-graft. While on both scaffolds, the bone neoformation started as early as 2 W (Fig. 1A), the frequency, maturation and quantity of newly formed bone were different depending on the associated biomaterial. The frequency of bone formation was higher when hBMSC were associated with TPB than HA/βTCP at 2 W, 4 W and 6 W post-graft (Fig. 1B). An increase of bone formation incidence with a rate reached 100% at 6 W was noted for TPB, whereas the bone incidence remained at the same level from 4 to 6 W for the HA/βTCP scaffold. Histological analysis of newly formed bone at 2 W, showed a beginning of bone formation with randomly oriented collagen fibrils on both biomaterials (Fig. 1A). Starting from 4 W, lamellar orientation was observed with osteoblasts lining the surface and osteocytes within the bone matrix. The newly formed lamellar bone was associated to bone marrow (BM) like elements. The quantification of new

Table 1
Primer sequences used in RT-qPCR.

Gene	Forward primer	Reverse primer
Mouse (m−)		
m-GAPDH (glyceraldehyde 3-phosphate dehydrogenase)	ACTGAGCAAGAGAGGCCCTA	TATGGGGGTCTGGGATGGAA
m-Ly6C (lymphocyte antigen 6C)	GCAGTGCTACGAGTGCTATGG	ACTGACGGGTCTTTAGTTTCCTT
m-Runx2 (runt-related transcription factor 2)	TTGACCTTTGTCCCAATGC	AGGTTGGAGGCACACATAGG
m-ALP (alkaline phosphatase)	TGTCTGGAACCGCACTGAACT	CAGTCAGGTTGTTCCGATTCAA
m-IBSP (bone sialoprotein 2)	ATGGAGACGGCGATAGTTCC	CTAGCTGTTACACCCGAGAGT
m-OC (osteocalcin)	AGGAGGGCAATAAGGTAGTGAA	TACCATAGATGCGTTTGTAGGC
m-CTR (calcitonin receptor)	GAGGTTCCTTCTCGTGAACAG	AGTCAGTGAGATTGGTAGGAGC
m-TRAP5b (tartrate-resistant acid phosphatase 5b)	CACTCCCACCCTGAGATTTGT	CATCGTCTGCACGGTTCTG
m-RANKL (receptor activator of nuclear factor kappa-B ligand)	CAGCATCGCTCTGTTCCTGTA	CTGCGTTTTCATGGAGTCTCA
Human (h−)		
h-GAPDH (glyceraldehyde 3-phosphate dehydrogenase)	CCAGCAAGAGCACAAGAGGA	GAGATTCAGTGTGGTGGGGG
h-Bax (BCL2-associated X protein)	GGAGGAAGTCCAATGTCCAG	GGGTTGTCGCCCTTTTCTAC
h-Bcl2 (B-cell leukemia protein-2)	CTGGTGGGAGCTTGCATCAC	ACAGCCTGCAGCTTTGTTTC
h-Runx2 (runt-related transcription factor 2)	GAATCCTCCACCCACCCAAG	AATGCTGGGTGGCCTACAAA
h-ALP (alkaline phosphatase)	CCACGTCTTCACATTTGGTG	GCAGTGAAGGGCTTCTTGTC
h-IBSP (bone sialoprotein 2)	CCATTCTGGCTTTGCATCCG	GGGACAAGAAGCCTATTACTTTGC
h-ON (osteonectin)	TGCCTGATGAGACAGAGGTG	TCCACCTGGACAGGATTAGC
h-OC (osteocalcin)	GTGCAGAGTCCAGCAAAGGT	TCCCAGCCATTGATACAGGT
h-OPN (osteopontin)	CGCAGACCTGACATCCAGTA	ATGGCCTTGTATGCACCATT
h-RANKL (receptor activator of nuclear factor kappa-B ligand)	ATCTGGCCAAGAGGAGCAAG	GACAGACTCACTTTATGGGAACC
h-SDF1 (stromal cell-derived factor 1)	CGCACTTTCACTCTCCGTCA	ATCGGCATGGGCATCTGTAG
h-PDGFb (platelet derived growth factor b)	TCCCGAGGAGCTTTATGAGA	TCATGTTCAGGTCCAACTCG
h-IGF1 (insulin like growth factor 1)	GCAGGAGGGACTCTGAAACC	CTGACATGGTATTTGGGGCCT

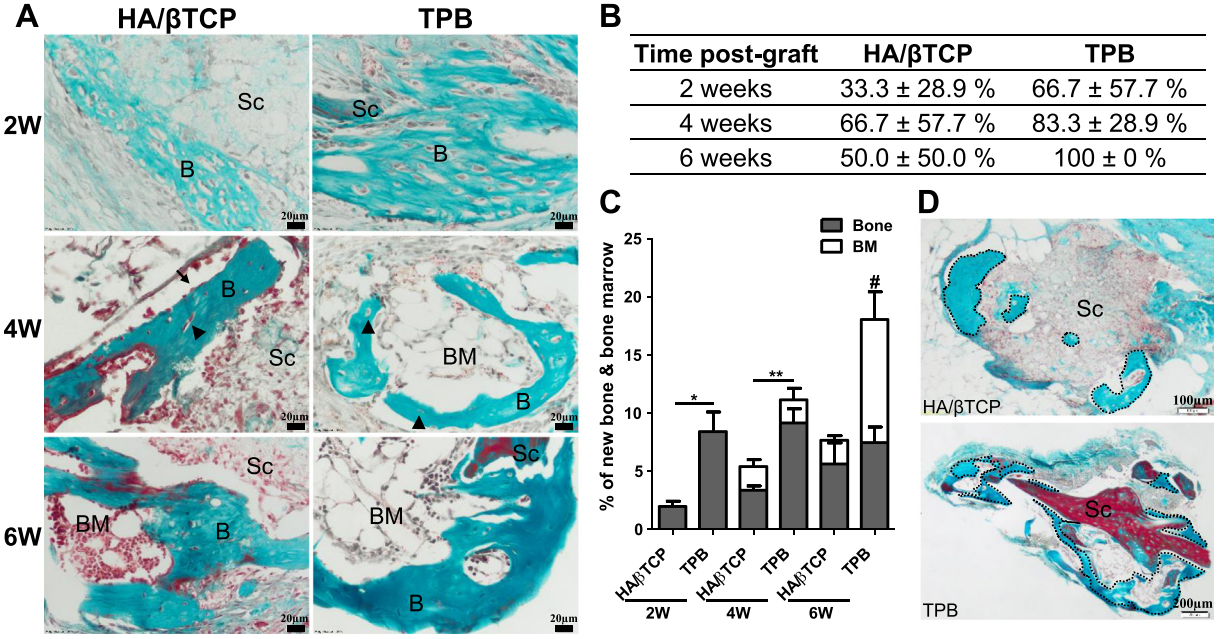


Fig. 1. Biomaterials impact on bone formation and maturation. (A) Masson's Trichrome staining of newly formed bone and BM-like elements 2, 4 and 6 weeks post-graft of hBMSC on HA/βTCP or TPB. Scale bar, 20 μm. Collagen and bone matrix are stained in green/blue; cytoplasm and erythrocytes in red; nuclei in purple/black. Arrows show osteoblasts lining the bone matrix. Arrow head show osteocytes within the bone matrix. B: bone; BM: bone marrow-like elements; Sc: scaffold. (B) Frequency of newly formed bone evaluated by Masson's Trichrome staining 2, 4 and 6 weeks post-graft and calculated as the ratio between the number of scaffolds with newly formed bone and the total number of implanted scaffolds (scaffolds with bone formation + scaffolds without bone formation) (mean ± SD). (C) Quantification of newly formed bone and BM-like elements 2, 4 and 6 weeks post-graft, using ImageJ software, expressed as a percentage of newly formed bone and BM area compared to the total implant area (mean ± SEM). $^{*}p < 0.05$, $^{**}p < 0.01$, is related to bone formation and $^{\#}p$ is related to bone marrow like elements formation (One way Anova test). (D) Histological analysis of newly formed bone localization on 2D sections of HA/βTCP and TPB, 6 weeks post-graft. The bone elements are surrounded by a dotted line. Sc: scaffold. Scale bar: 100 μm for HA/βTCP, 200 μm for TPB. (For interpretation of the references to colour in this figure legend, the reader is referred to the web version of this article.)

bone and BM (Fig. 1C) revealed that the bone quantity was dependent on the associated biomaterial. As soon as 2 W the bone quantity was 4 times higher on TPB than on HA/βTCP (8.4% *vs* 2.0%), stilled 2.7 times higher at 4 W (9.1% *vs* 3.4%) and became similar at 6 W (7.4% *vs* 5.6%) (Fig. 1C). BM like elements appeared 4 W post-graft on both biomaterials (2.0% *vs* 2.0%) and were significantly higher at 6 W on TPB than on HA/βTCP scaffold (10.6% *vs* 2.0%) (Fig. 1C). The localization of newly formed bone was evaluated on 2D sections. Our results showed a homogeneous distribution of new bone which surrounded and bridged TPB trabeculae

(Fig. 1D, bottom). In contrast, only 17.5% of HA/βTCP sections presented new bone formation in both the inner and the outer area of this biomaterial (Fig. 1D, top).

3.2. Cell persistence on the graft site depends on the associated biomaterial

The number of hBMSC present on the grafted scaffold at different time post-implantation *in vivo* was quantified by qPCR using a human-specific assay [34]. The cell number was compared to time 0 (T0 = 10^6 hBMSC). Only 43 ± 2% of the initially grafted cells were found on HA/βTCP at 24 h ($p < 0.001$) whereas 80 ± 10% of them were still present on TPB ($p < 0.05$) making the number of adherent hBMSC significantly higher on TPB compared to HA/βTCP ($p < 0.001$; Fig. 2A). This difference remained during the first week post-implantation (31 ± 5% *versus* 74 ± 11% at 48 h; $p < 0.001$ and 35 ± 3% *versus* 83 ± 18% at 1 W; $p < 0.01$ for HA/βTCP and TPB, respectively). After 2 W, the cell number decreased gradually on TPB comparing to T0 ($p < 0.01$) but were still significantly higher than on HA/βTCP at 4 W (57 ± 4% *versus* 34 ± 4%; $p < 0.01$). On HA/βTCP, no more decrease was observed after 24 h post-implantation. Interestingly, about 30% of grafted cells (HA/βTCP: 30 ± 4%; TPB: 34 ± 8%) persisted until 6 W on both biomaterials. The presence of grafted hBMSC on the associated biomaterial was confirmed by immunohistochemical staining of human anti-lamin AC at 24 h post-graft (Fig. 2B). Positive cells were essentially found on the outer surface of both biomaterials.

3.3. Cell disappearance is associated to their migration into the adjacent tissues

Cell loss on HA/βTCP did not appear to be due to a higher apoptosis as mRNA ratio of human Bax (pro-apoptotic factor) to Bcl-2 (anti-apoptotic factor) did not differ during 72 h between both biomaterials (Fig. 3A). Despite an increase of this ratio at 24 h on both biomaterials in comparison with T0 ($p < 0.001$), a rapid decrease to a basal state was observed at 72 h and cell death was not induced as shown by the absence of TACS® labelling (Fig. 3B). Cells around both biomaterials were negative for TACS® staining reflecting the absence of apoptosis and were not swollen demonstrating neither necrosis. These results were confirmed at 48 and 72 h post-graft (data not shown). Only rare apoptotic cells were found a distance from the biomaterials, in fibrotic tissue at 24 h (Fig. 3C). We then hypothesized that the decline in cell number is due to an increased inflammatory microenvironment on HA/βTCP. As shown in Fig. 3D, the mRNA expression of the mouse pro-inflammatory marker mLy6C was independent of the associated biomaterial and of grafting human cells 24 h after subcutis implantation. A significant decrease of expression was observed at 48 h on both biomaterials when associated with human cells (HA/βTCP: $p < 0.01$ and TPB: $p < 0.001$) and this diminution persisted until 1 W (HA/βTCP: $p < 0.01$ and TPB: $p < 0.001$). As MSC have the ability to migrate to several organs after systemic administration [36] we decided to assess the biodistribution of human cells in the host mice. Analysis using a human-specific qPCR assay did not found hBMSC in organs like heart, kidney, spleen, liver and lung neither at 24 or 48 h nor from 1 W to 6 W post-implantation (data not shown). Interestingly, human cells were found in skin and muscle adjacent to the implanted biomaterials (Fig. 3E). At 24 h, hBMSC migration on adjacent tissues (skin + muscle) was significantly higher when cells were seeded on HA/βTCP than on TPB ($p < 0.05$). At 48 h, hBMSC were still detected in skin and muscle without any difference between both scaffolds. At 1 W, few transplanted cells were found on adjacent tissues regardless of scaffolds, then human cells totally disappeared from surrounding tissues at 2 W (Fig. 3E).

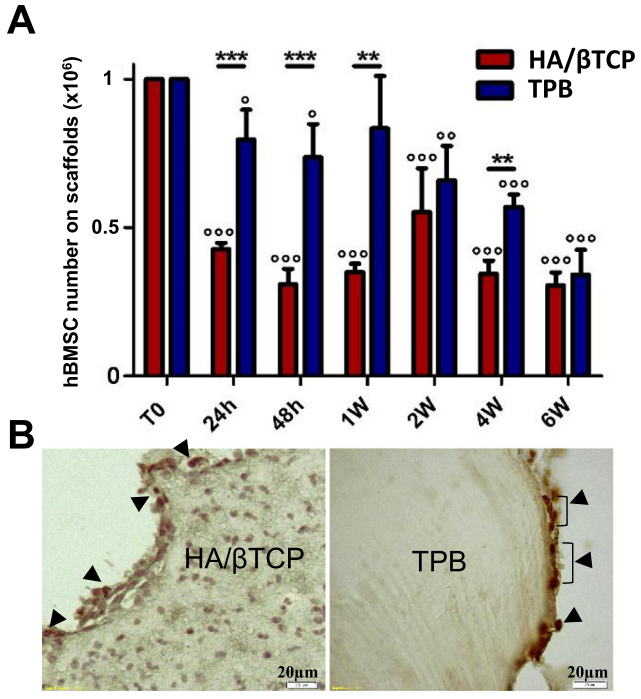


Fig. 2. Biomaterials impact on hBMSC persistence on the graft site. (A) Evaluation of hBMSC number on HA/βTCP and TPB, from T0 to 6 W post-graft, using human-specific qPCR assay. (B) Immunohistochemical staining of human lamin AC showing grafted hBMSC (dark brown staining) at 24 h. Black arrowhead indicate the cells positive for the lamin AC staining. Scale bar: 20 µm. (For interpretation of the references to colour in this figure legend, the reader is referred to the web version of this article.)

3.4. Human BMSC adhesion is impacted by the associated biomaterial

As *in vivo* results showed differences on the number of survival and/or adherent hBMSC, we decided to evaluate the impact of biomaterials on cell adhesion by *in vitro* analysis. After 3 h of cell incubation with each kind of biomaterial, total DNA labelled with Picogreen solution was quantified by spectrophotometry. The proportion of adherent cells on TPB was 49 ± 18% whereas on HA/βTCP it was only 28 ± 22% ($p < 0.01$; Fig. 4A). As the roughness and the structure of biomaterials may impact the cell adhesion and distribution, SEM analysis was conducted on both scaffolds 3 h post-seeding (Fig. 4B). On HA/bTCP, cells adhered on the outer surface and surprisingly are not localized on the grove part. In contrast, an important number of hBMSC invaded the open pores of TPB. Whereas most of the cells exhibited on both scaffold a ball-shaped morphology with some starting to induce cytoplasmic extension indicating beginning of cell adhesion, we observed only on TPB the presence of flat cells with high cytoplasmic extensions indicating their early and tight adhesion on TPB (Fig. 4B, white arrows).

3.5. Biomaterial characterization

To understand differences of cell behavior we characterized the synthetic HA/βTCP ceramic and the human allogeneic bone TPB scaffolds by SEM, XRD and FTIR spectroscopy. SEM analysis illustrated that the biomaterial granules have similar size and weight (Fig. 5A, top) as specified in materials and methods. The macroporosity of the HA/βTCP granule was poor in comparison to the open and interconnected porosity of the trabecular structure in TPB. At high magnification (Fig. 5A, bottom), the surface of HA/βTCP was highly micro porous due to the incomplete sintering of the ceramic. The TPB scaffold exhibited a surface composed of aligned

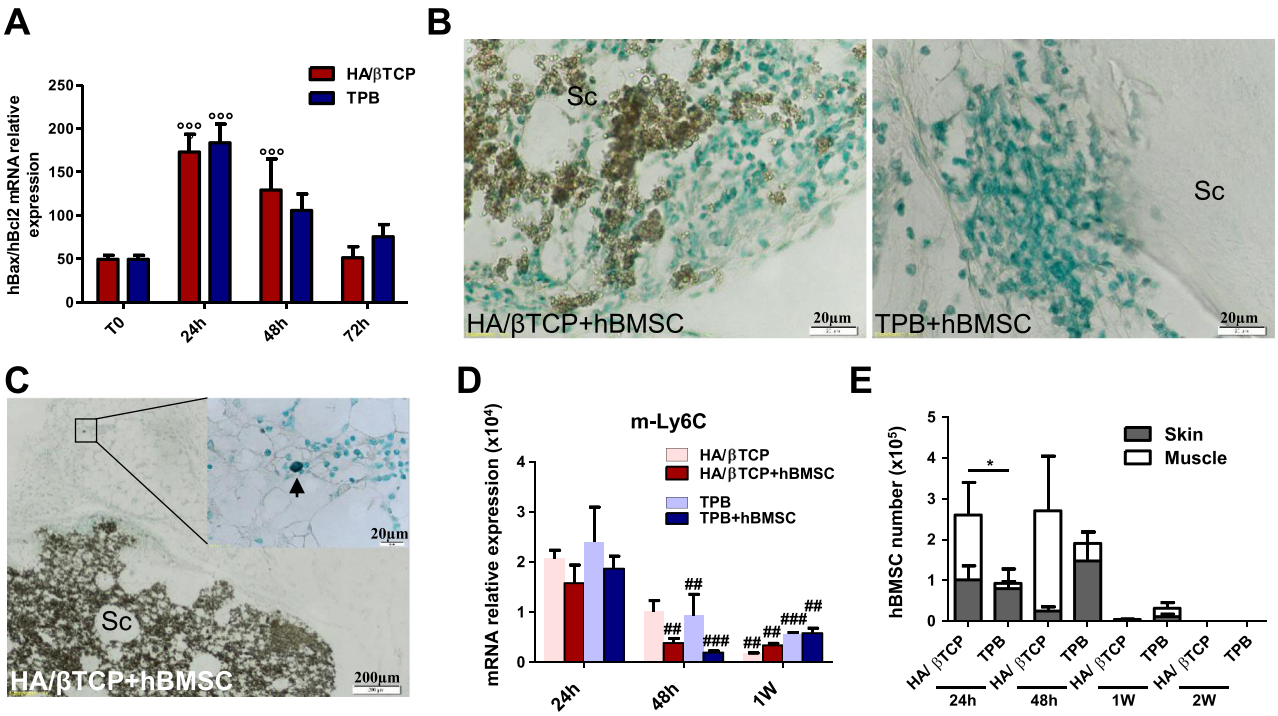


Fig. 3. Cell disappearance is associated to their migration into the adjacent tissues. (A-B) Apoptotic cells staining in situ by TACS® kit 24 h post-graft. (A) Non-apoptotic cells are totally blue and not enlarged. HA/βTCP and TPB associated with hBMSCs, 24 h post-graft. (B) Positive cell in fibrotic tissue around HA/βTCP at 24 h: apoptotic cells exhibit dark nuclear staining and enlarged shape reflect a beginning of necrosis (arrow). (C) Apoptosis detection through hBAX/hBCL-2 mRNA ratio as determined by RT-qPCR using human-specific primers 24, 48 and 72 h post-graft. (D) mRNA expression of mouse pro-inflammatory factor Ly6C (m-Ly6C) as determined by RT-qPCR using mouse-specific primer was normalized to GAPDH and presented as mRNA relative expression ($2^{-\Delta Ct(m\text{-}Ly6C-GAPDH)}$) 24 h, 48 h and 1 W post-graft. (E) Analysis of hBMSC migration in adjacent tissues (skin and muscle) to implanted biomaterials at 24 h, 48 h, 1 and 2 W using human-specific assay by qPCR. Data are represented as mean ± SEM.; °p < 0.05, °°p < 0.01, °°°p < 0.001 when compared to T0 and #p when compared to 24 h; *p when HA/βTCP compared to TPB. Two way ANOVA test for Fig. 3C–D and Mann-Whitney test for Fig. 3E. (For interpretation of the references to colour in this figure legend, the reader is referred to the web version of this article.)

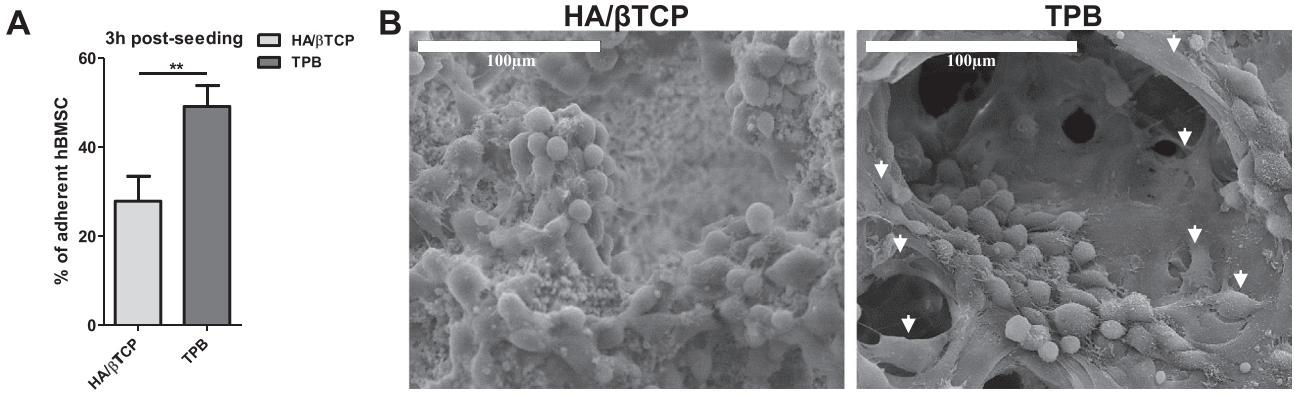


Fig. 4. Adherence of h-BMSCs *in vitro*. (A) Ratio of adherent hBMSC on HA/βTCP and TPB was evaluated *in vitro* 3 h post-seeding by spectrophotometry using Picogreen labelling. (B) Analysis of hBMSC adherence and shape by Scanning Electron Microscopy (SEM) 3 h post-seeding on biomaterials. White arrow indicate the flat adherent cells.

mineralized collagen fibers. XRD analysis of the synthetic scaffold indicated narrow and intense diffraction peaks typical of the highly crystalline HA and β-TCP phases in the weight ratio of 65/35 while the XRD pattern of TPB corresponded to an amorphous or nano-crystalline hydroxyapatite phase typical of human bone (Fig. 5B). FTIR spectroscopy corroborated these findings with PO_4 peaks around 600 and 1050 cm^{-1} corresponding to HA and β-TCP compounds. The FTIR spectrum of TPB indicated additional amide I and II bands around 1680 cm^{-1} which are typical of the collagen proteins (Fig. 5C). The structure of scaffolds was analyzed by micro-CT (Fig. 5D). The volume of HA/βTCP was higher than TPB ($p < 0.01$) whereas the surface area was similar between both biomaterials. Interestingly, the open porosity was significantly higher on TPB and consists of 85.6 ± 5.8% of open pores whereas the open porosity was 28.4 ± 3.4% for the HA/βTCP material ($p < 0.01$; Fig. 5E). These results suggest that a higher open porosity and interconnectivity in the TPB scaffold may have favored cell adhesion in comparison to the synthetic HA/βTCP biomaterial.

3.6. Osteoblastic gene expression by hBMSC is impacted by their seeding on a 3D scaffolds in vitro

As biomaterials impact cell morphology, their influence on osteoblastic gene expression was assessed (Fig. 6). Cells were seeded on each biomaterial for 24 h (n = 3 donors) and 1 W (n = 5 donors) and mRNA expression of osteoblastic genes was compared to T0 (cells cultured on 2D flasks). At 24 h, only osteopontin (OPN) was up-regulated and tend to be higher when cells are grafted on

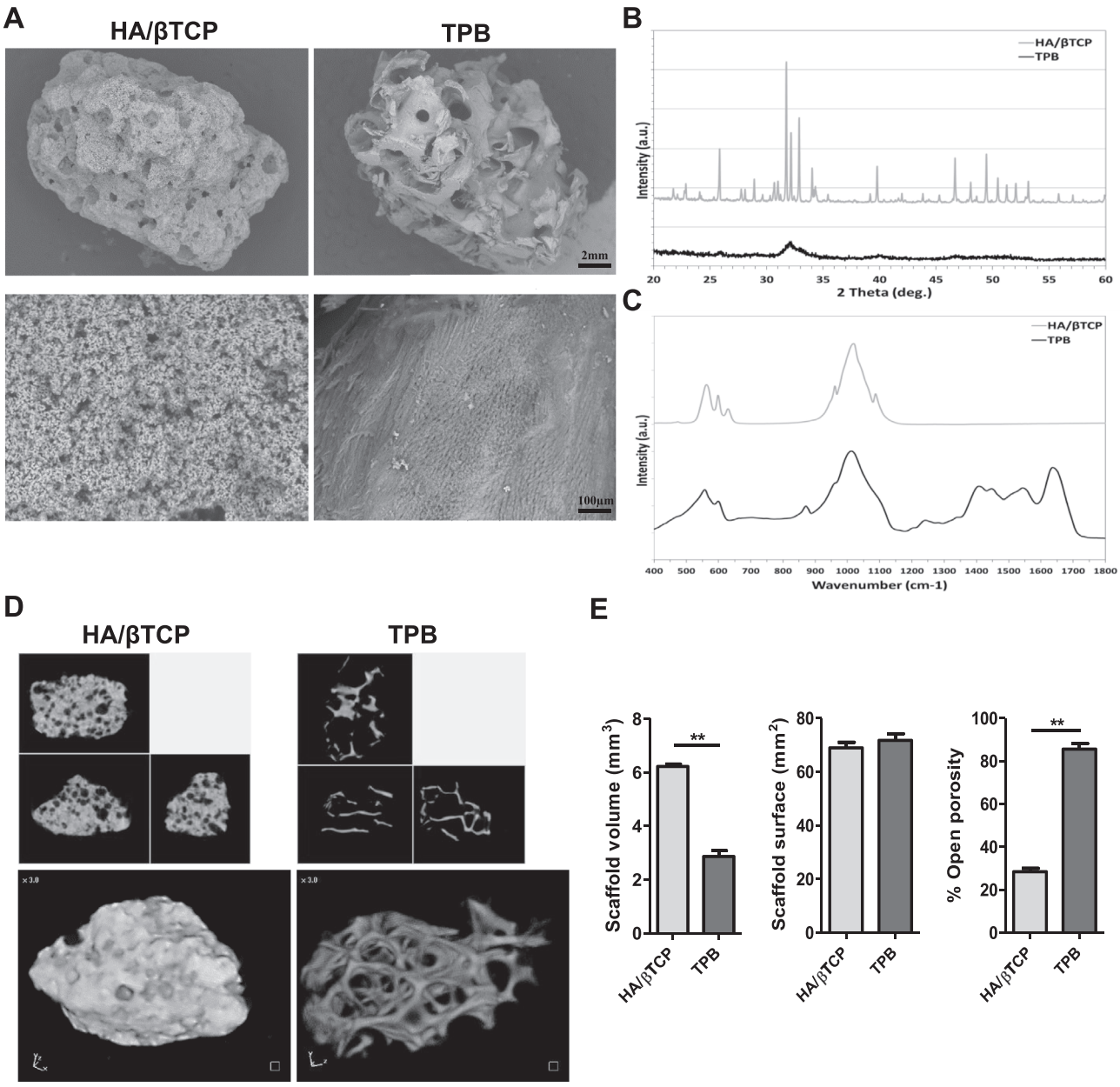


Fig. 5. Biomaterials properties. (A) The porosity and the interconnectivity of both scaffolds were evaluated by Scanning Electron Microscopy (SEM), at low (top) and high magnifications (bottom). (B) X-ray diffraction (XRD) characterization of biomaterials phases and crystallinity. (C) Fourier Transform Infrared Spectroscopy spectra of biomaterials. (D) Micro computed-tomography (µCT) images of biomaterials (top) and 3D reconstruction by stacking all the 2D cross-sections (bottom). (E) Measurement of morphometric parameters of biomaterials by µCT. Data are represented as mean ± SEM. $^{**}p < 0.01$. Mann-Whitney test.

HA/βTCP compared to TPB. At 1 W, whereas the early osteoblastic factor Runx2 was slightly induced, intermediate (OPN, osteonectin [ON]) and late (h-IBSP and osteocalcin [OC]) osteoblastic genes were enhanced. A higher expression of ON and OPN was observed when cells were grafted on HA/βTCP whereas IBSP was preferentially induced on TPB. No difference was seen for OC and surprisingly, mRNA expression of ALP, was down-regulated. Taken together, these results showed that the 3D loading induces hBMSC to differentiate and express osteoblastic genes with a different manner depending on the biomaterial.

3.7. Grafted hBMSCs play a direct role in bone formation and are impacted by the nature of the scaffold

As biomaterial induce osteoblastic gene expression *in vitro* and because grafted hBMSC persist until 6 W *in vivo* we decided to evaluate their direct and paracrine contribution among time *in vivo*. Expression of osteoblastic genes was analyzed by RT-qPCR using human-specific primers (Fig. 7A). The expression of human Runx2 (h-Runx2), an early osteoblastic gene was evaluated starting from 48 h post-graft. Our results showed an up-regulation at 2 W comparing to T0 on both biomaterials (TPB: $p < 0.001$; HA/βTCP: $p < 0.05$) and was higher on TPB in comparison to HA/βTCP ($p < 0.01$). This up regulation remains higher on TPB at 4 and 6 W ($p < 0.001$; Fig. 7A). The late osteoblastic genes h-IBSP and h-OC were significantly up-regulated from 2 W on TPB in comparison to T0 and their expression increased overtime (h-IBSP: $p < 0.05$ at 2 W; $p < 0.001$ at 4 and 6 W. h-OC: $p < 0.01$ at 2 and 4 W; $p < 0.001$ at 6 W). OC expression becomes significantly expressed only at 6 W on HA/βTCP ($p < 0.001$; Fig. 7A). In contrast to these 3 genes, h-OPN is found to be significantly more expressed at 4 W on HA/βTCP and becomes significantly expressed on TPB only

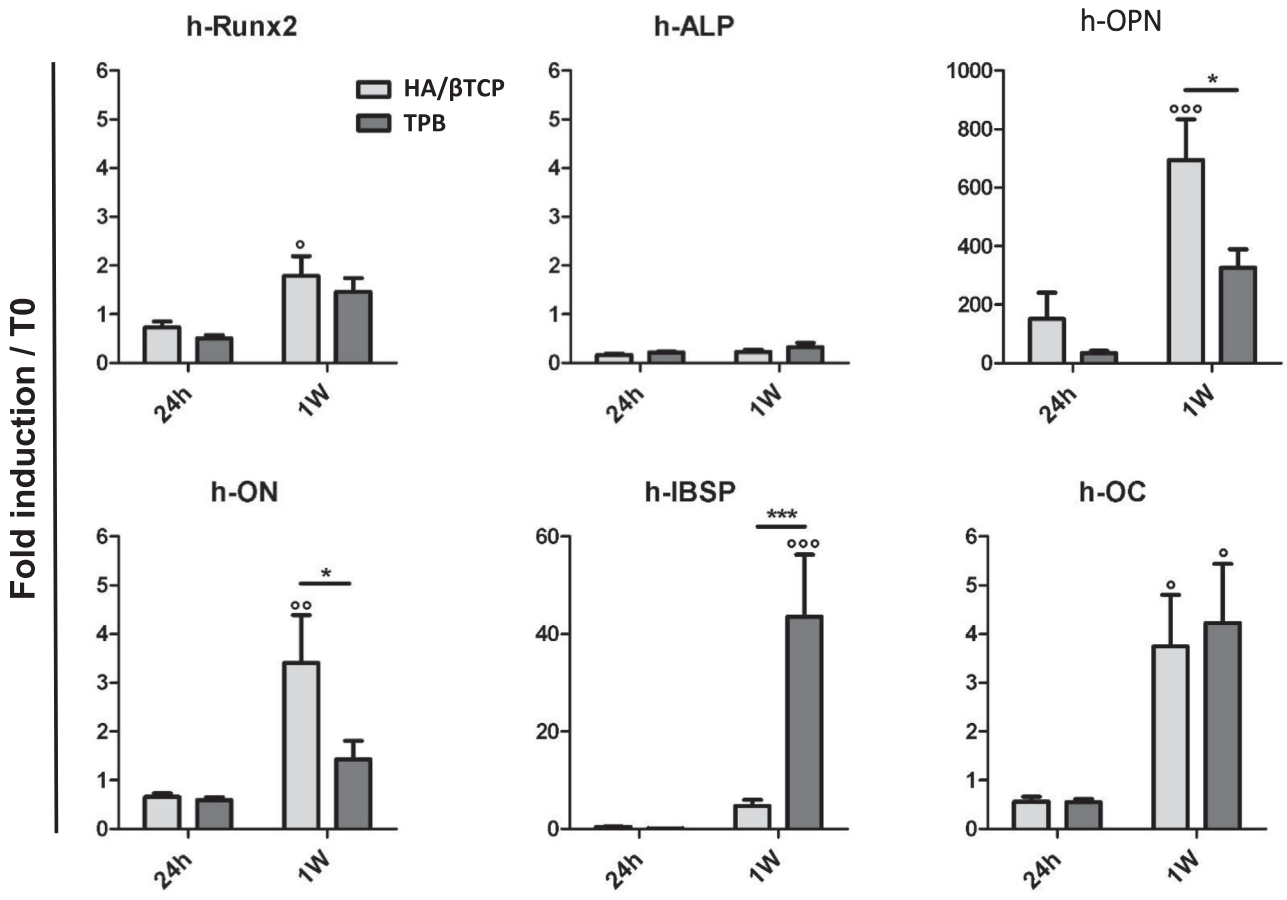


Fig. 6. Osteoblastic gene expression by h-BMSCs seeded on 3D biomaterials *in vitro*. mRNA expression of human Runx2, ALP, OPN, ON, IBSP, and OC was determined by RT-qPCR using human-specific primers. hBMSC seeded on biomaterials (3D) for 24 h and 1 W were compared to hBMSC before seeding (T0 = cells cultured on 2D flasks). All genes were normalized to GAPDH (ΔCt) and to the gene expression for hBMSC at T0 and presented as $2^{-\Delta\Delta Ct(\text{fold induction 3D/T0})}$). Data are represented as mean ± SEM. °p < 0.05, °°p < 0.01, °°°p < 0.001 when 1 W compared to 24 h and *p when HA/βTCP compared to TPB. Two way ANOVA test.

at 6 W ($p < 0.05$; Fig. 7A). To confirm the direct contribution of hBMSC in bone formation, immunofluorescent detection of human IBSP (h-IBSP) protein using a specific antibody was performed at 4 W. On both biomaterials, newly formed bone showed positive areas for h-IBSP confirming the direct contribution of human cells on bone formation (Fig. 7B). The quantification of the proportion of positive surfaces indicated that h-IBSP represent around 15–20% of the total bone surface area and was not different between both biomaterials (Fig. 7C).

3.8. Grafted hBMSC exert a paracrine effect

As some regions of newly bone did not expressed h-IBSP, we supposed that host cells also contribute to bone formation. In order to verify this hypothesis, we analyzed mouse osteoblastic gene expression using mouse-specific primers. Mouse IBSP, OC and ALP were expressed only when biomaterials were associated with hBMSC with a higher expression of m-IBSP and m-ALP at 4 W when cells were grafted on HA/βTCP ($p < 0.05$ and $p < 0.001$ respectively, Fig. 8A). In contrast to human genes, m-Runx2 was not expressed even if hBMSC were grafted on biomaterials. As these results suggest that hBMSC induce host cells chemoattraction, we decide to determine which chemokines are involved in this mechanism. Using human-specific primers, we analyzed gene expression of SDF1, PDGFb and IGF1 known as factors involved in MSC recruitment [19]. Surprisingly, SDF1 and PDGFb were not expressed by grafted hBMSC throughout the 6 W (Fig. 8B). However, IGF1 expression was increased about 5 times as early as 24 h and reach a peak at 4 W on TPB ($p < 0.001$ *vs* T0) and 6 W on HA/βTCP ($p < 0.001$ *vs* T0). Taken together, these results indicate that chemoattraction of murine cells may involve IGF1.

3.9. Osteoclastic activity induced by hBMSC is impacted by the associated scaffold

In parallel to osteoblastic lineage, osteoclasts are critical to enhance bone formation [38]. We then assessed the impact of biomaterials on osteoclastic activity by an enzymatic staining for TRAP. $TRAP^+$ cells appeared on both biomaterials 2 W post-graft of hBMSC whereas they were absent on controls at the same time (Fig. 9A). On HA/βTCP, $TRAP^+$ cells were found all around the biomaterial in contact with the outer surface area, frequently fused in a wide cell network and only some of them were found in inner macropores. On TPB, $TRAP^+$ cells around predominantly areas with small surfaces and were sparsely distributed only in certain parts of this biomaterial (Fig. 9A). Quantitatively, 2 W post-graft the ratio of HA/βTCP outer surface area covered by $TRAP^+$ cells was 8-fold higher than on TPB (10.69 ± 1.72% *versus* 1.38 ± 0.28%, $p < 0.001$) (Fig. 9B). These data were confirmed by RT-qPCR analysis of mouse osteoclastic markers m-CTR and m-TRAP5b. Relative

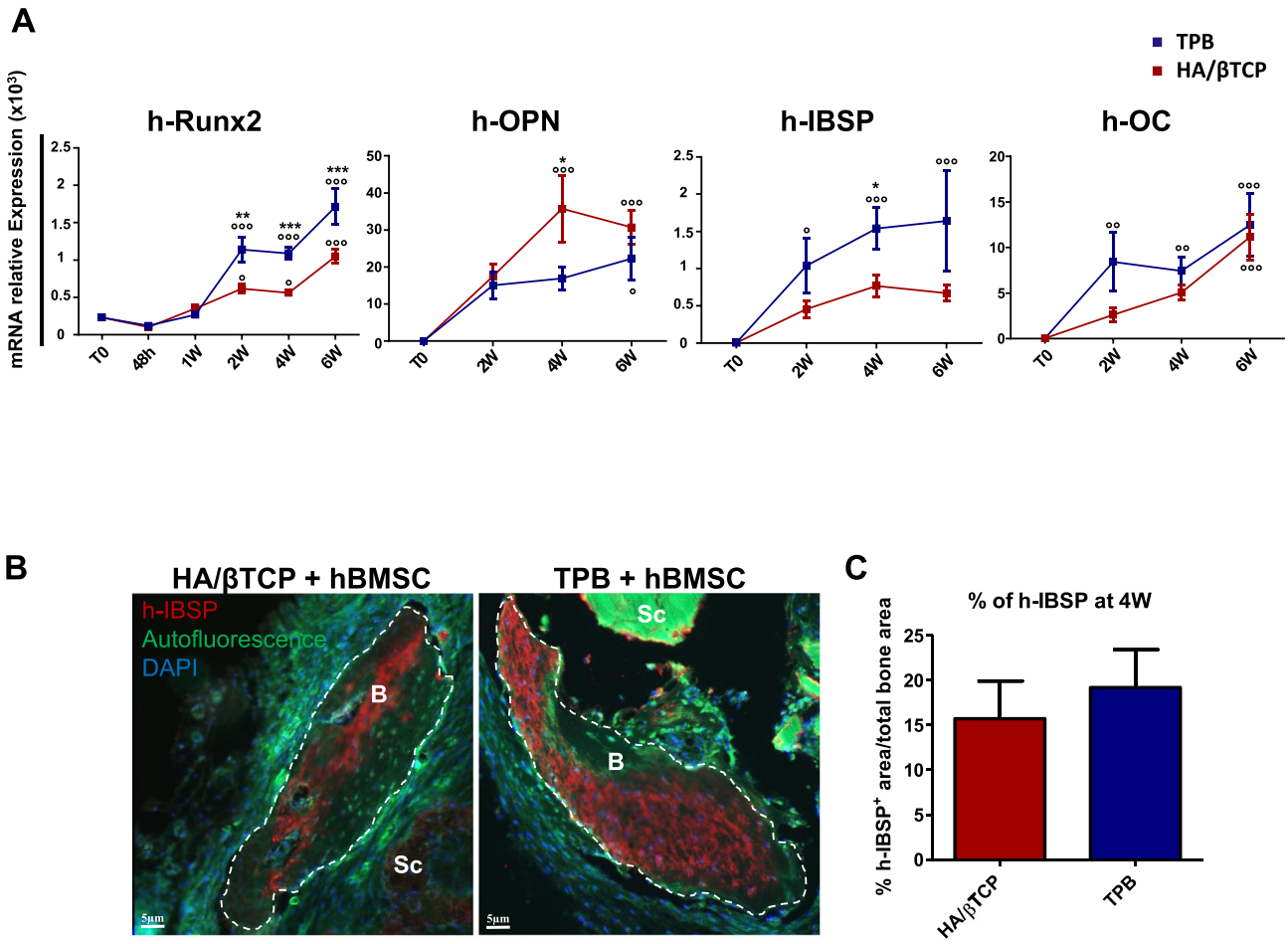


Fig. 7. Direct contribution of grafted hBMSC in bone formation. (A) Human osteoblastic gene expression (h-RUNX2, h-OPN, h-IBSP, h-OC) was determined by RT-qPCR using human-specific primers, from 48 h to 6 W post-implantation for h-Runx2 and at 2, 4 and 6 W for h-OPN, h-IBSP and h-OC. (B) Immunofluorescent labelling of human IBSP (hIBSP) at 4 W. New formed bone is delimited by white dotted line, h-IBSP positive areas are labelled in red and nucleus in blue. Bone matrix, scaffolds and fibrous tissues are autofluorescent in green. (C) Quantification of h-IBSP positive area after immunofluorescent staining at 4 W. (For interpretation of the references to colour in this figure legend, the reader is referred to the web version of this article.)

expression of studied genes was induced by hBMSC on both biomaterials ($p < 0.001$) with a higher expression on HA/βTCP ($p < 0.001$ for m-CTR and $p < 0.01$ for m-TRAP5b) (Fig. 9C). Taken together, these results show a higher osteoclastic activity on HA/βTCP than on the TPB scaffold.

As osteoclastogenesis is regulated primarily by RANKL secreted by MSC and osteoblasts [38], we evaluated by RT-qPCR mRNA expression of this cytokine in human grafted cells and in mouse cells. Human RANKL (h-RANKL) expression increased starting from 24 h post-graft on both biomaterials and became significantly up-regulated compared to T0 at 1 W on HA/βTCP and later, at 2 W on TPB ($p < 0.01$). In addition to be faster up-regulated, h-RANKL was significantly more expressed at 2 W on HA/βTCP compared to TPB ($P < 0.01$; Fig. 9D). The presence of hBMSC impacted mouse RANKL (m-RANKL) mRNA expression only on HA/βTCP in comparison to control ($p < 0.001$; Fig. 9E). As for h-RANKL, m-RANKL mRNA was expressed at a higher level when hBMSC were grafted on HA/βTCP ($p < 0.001$; Fig. 9E). To confirm the impact of the biomaterial on h-RANKL expression, *in vitro* experiments were performed. First, while no expression of h-RANKL was observed on 2D (T0), we notice an up-regulation at 24 h on both biomaterials ($p < 0.001$; Fig. 9F). This expression was significantly higher on HA/βTCP comparing to TPB ($p < 0.001$). Then, mRNA expression of h-RANKL decreased and it was almost undetectable at 1 W on HA/βTCP and on TPB (HA/βTCP: $p < 0.001$; TPB: $p < 0.01$; Fig. 9F).

4. Discussion

Tissue engineering using BMSC transplantation associated with biomaterials is one of the most promising strategies for 3D bone reconstruction [26]. Biomaterials provide a niche for progenitor differentiation and bone neoformation guidance [39]. However, scaffold diversity is a source of heterogeneity on bone formation efficiency [9,10,31,33]. The aim of our project was to understand the causes of this heterogeneity during bone regeneration. To this end, we compared two scaffolds already used clinically and that differ by their structure and composition: the synthetic HA/βTCP and the biologic TPB.

Using an ectopic model our results confirmed that biomaterials impact bone neoformation [9] with only 50% of HA/βTCP scaffolds yielding bone formation, *versus* 100% of TPB at 6 W. Moreover, bone quantity was higher on TPB at 2 and 4 W. In both cases, bone formation first undergoes endochondral phases followed by lamellar bone orientation, which mimic the kinetics of physiological fracture repair [3]. However, bone maturation was more rapid on

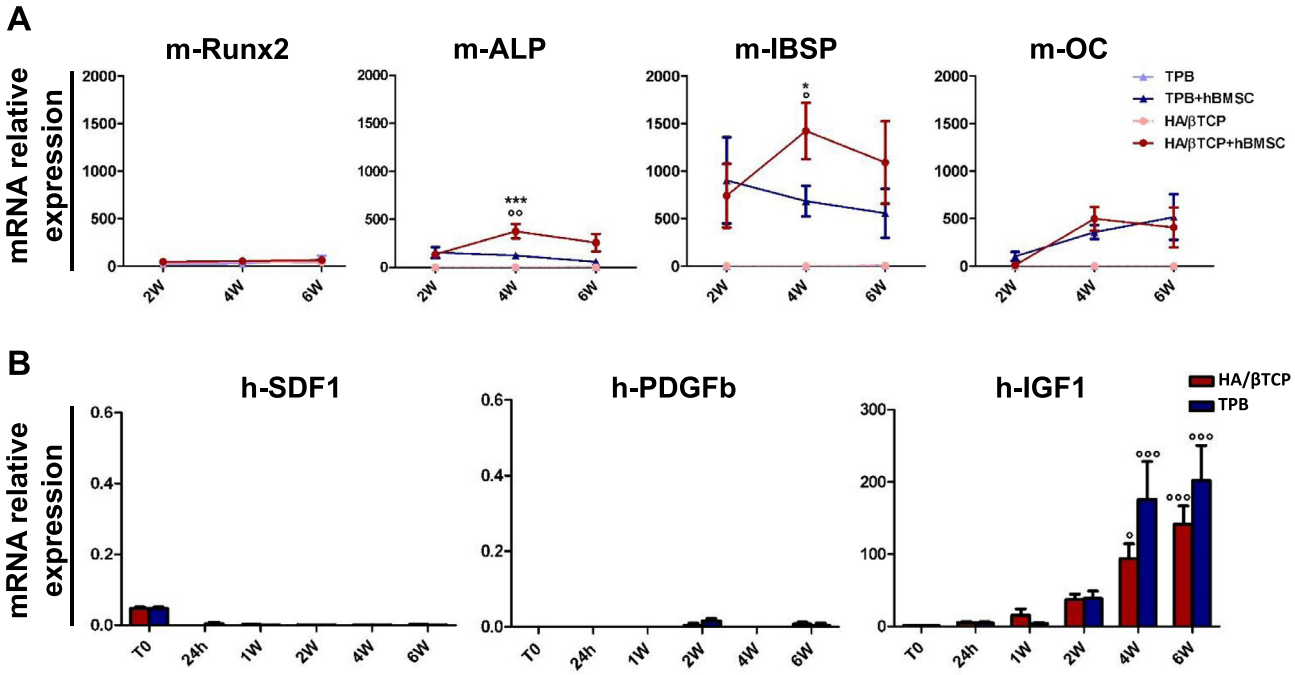


Fig. 8. Paracrine contribution of grafted hBMSC in bone formation. (A) Mouse osteoblastic gene expression (m-RUNX2, m-IBSP, m-OC, m-ALP) on biomaterials alone and biomaterials associated with hBMSC was determined by RT-qPCR using mouse-specific primers, between 2 and 6 W post-implantation. (B) Human chemokine gene expression (SDF-1, PDGFb, IGF1) was determined by RT-qPCR using human-specific primers, at 24 h then at 1, 2, 4 and 6 W post-implantation. Values for all genes were normalized to GAPDH of corresponding species and results are presented as $2^{-\Delta Ct}$. Data are represented as mean ± SEM. $^{*}p < 0.05$, $^{**}p < 0.01$, $^{***}p < 0.001$ when HA/βTCP compared to TPB and °p when compared to T0. Two way ANOVA test.

TPB as shown by an early onset of lamellar bone organization and by a higher proportion of BM-like elements at 6 W. Our results are strengthened by a study showing that on HA/βTCP hematopoiesis and therefore bone maturation begins late, around 7 W post-graft [17].

As we previously showed that bone formation can be related to hBMSC number [34], we count cells present on grafted scaffolds at different time post-transplantation. Interestingly, as early as 24 h post-graft more than 50% of initially grafted cells disappeared on HA/βTCP *versus* only 20% on TPB. Cell loss was not due to a higher apoptosis or inflammation on HA/βTCP but to an increase of grafted hBMSC migration to adjacent tissues like skin and muscle. Contrary to systemic administration [37], we confirmed that cells loaded on biomaterials did not migrate further into organs like heart, kidney, spleen, liver or lung which is an important safety consideration to initiate clinical trials [34,36]. Moreover, migrated cells on adjacent tissues disappeared after 1 W, probably by a local inflammation or by anoikis (apoptosis induced by loss of cell anchorage) [40], whereas they were still present until 6 W on biomaterials reflecting a better microenvironment to their survival. Lower cell migration from TPB was due to their higher seeding efficiency on this scaffold as showed by *in vitro* analysis. Despite the same surface area and macropores size >100 μm that represent appropriate conditions for cell adhesion [31], we showed that TPB presents a higher accessible surface area for cell invasion as it is composed of 85% of open pores. Our *in vitro* and SEM analysis confirmed that this property favors hBMSC attachment, fast spreading and allows their physical contact by cytoplasmic extensions [31]. Furthermore, TPB present numerous flat areas similar to natural endosteum structure where MSC preferentially attach [41]. The spongy architecture of TPB represents a better conformation to guide new bone formation compared to the single bloc structure of HA/βTCP. In addition, the high level of closed pores on HA/βTCP concentrate cell adherence on the outer surface area [30] and can hinder new bone invasion which may explain the major bone formation around the peripheral perimeter. Beyond the structural advantage of TPB, chemical composition and in particular the presence of collagen fibers as shown by our SEM and FTIR analysis could promote hBMSC adhesion. This is supported by previous *in vitro* study which noted that the better cell adhesion is obtained on support containing collagen fibers [31].

In addition to the impact on cell attachment and morphology, biomaterials influence MSC osteogenic potential [9,10]. We then focused on hBMSC behavior *in vitro* and during bone regeneration *in vivo*. *In vitro* analysis confirmed that cell seeding on 3D carriers induces osteoblastic gene expression variably depending on the scaffold [9]. At 1 W, ON and OPN were more expressed on HA/βTCP whereas IBSP was increased on TPB. These results can be explained by different kinetics of osteoblastic marker regulation. ON and OPN are known to be induced before IBSP [42] so we cannot exclude their higher expression on TPB between 24 h and 1 W. The increased IBSP expression on TPB at 1 W may reflect that hBMSC are more engaged in osteoblastic differentiation than on HA/βTCP [43]. Morphology of hBMSC 3 h post-seeding on scaffolds support this hypothesis as the elongated shape of adherent cells on TPB may promote their osteogenic potential contrary to round cells on HA/βTCP [44]. Taken together, our results indicated that the 3D seeding induces osteoblastic commitment of hBMSC but in different manner depending on the used biomaterial. However, the absence of osteoblastic gene induction at 24 h suggests an autocrine regulation of hBMSC differentiation in addition to a direct effect of biomaterials.

In vivo, hBMSC expressed the osteoblastic genes (Runx2, OPN, IBSP and OC) when grafted on biomaterials. Their expression increased and persisted over time which reflects cell survival and differentiation, indicating the direct contribution of the grafted hBMSC in bone formation. Human OPN and IBSP genes code for proteins from the "Small Integrin-Binding Ligand N-linked Glycoproteins (SIBLING)" family and are differently regulated depending on the nature of the scaffolds. These *in vivo* results, with an earlier

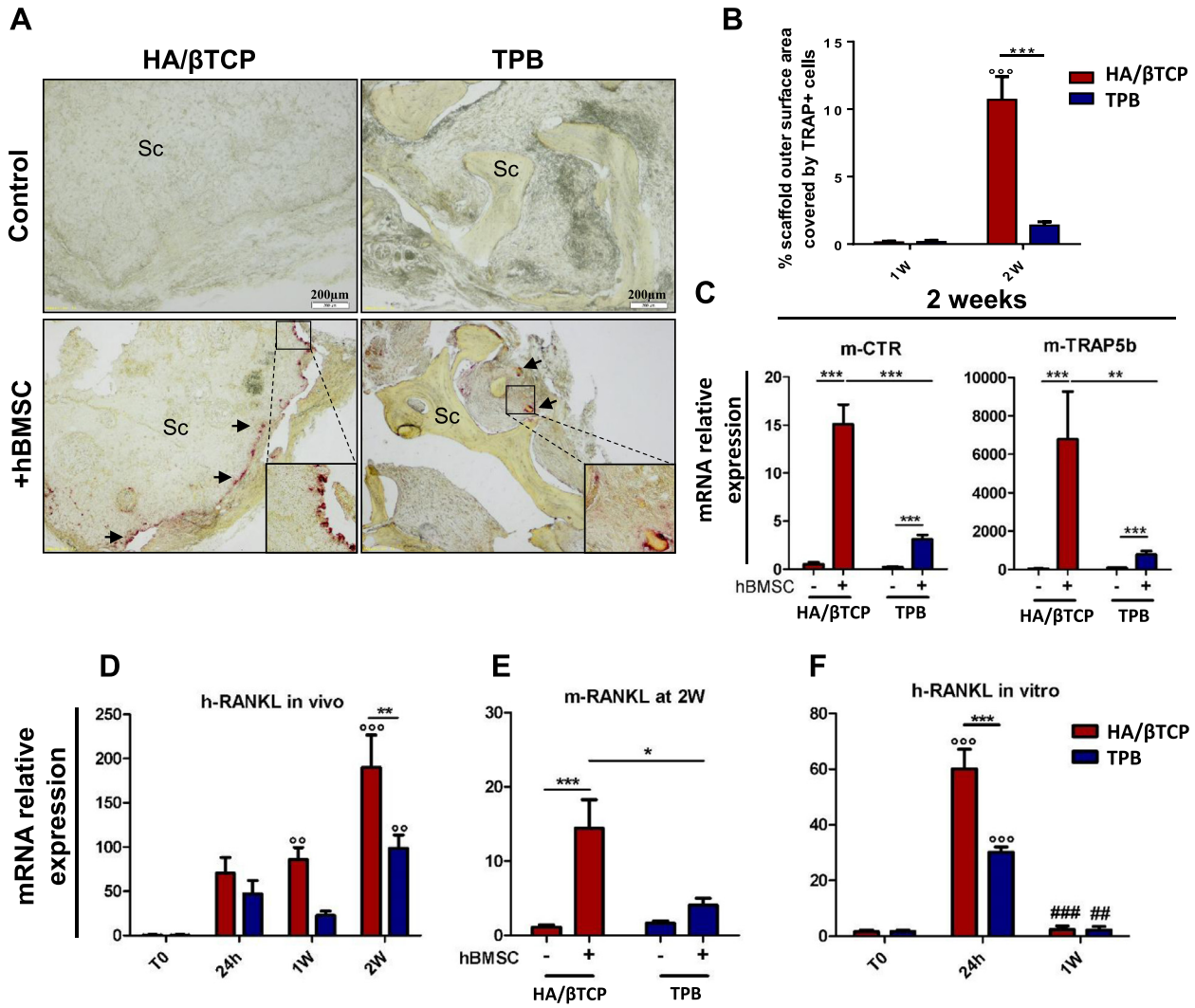


Fig. 9. Biomaterials impact on osteoclastic activity. (A) Tartrate-resistant acid phosphatase (TRAP) staining of osteoclasts (arrows) 2 W post-graft on biomaterials alone (control) and associated with hBMSC (+hBMSC). Sc: scaffold. Scale bar = 200 μm. (B) Rate of scaffold outer surface area covered by TRAP positive cells at 1 and 2 W post-graft on biomaterials associated with hBMSC. (C) Mouse osteoclastic gene expression (m-CTR, m-TRAP5b) on biomaterials alone (−) and associated with hBMSC (+) was determined by RT-qPCR using mouse-specific primers, at 2 W post-implantation. (D) mRNA relative expression of human RANKL (h-RANKL) was evaluated at T0 and at 24 h, 1 and 2 W post-graft of biomaterials associated with hBMSC. (E) mRNA relative expression of mouse RANKL (m-RANKL) was evaluated at 2 W post-graft of biomaterials alone (−) and associated with hBMSC (+). (F) mRNA relative expression of human RANKL (h-RANKL) was evaluated *in vitro* at T0 (2D) and at 24 h and 1 W after seeding of hBMSC on biomaterials. Values for all genes were normalized to GAPDH and results are presented as $2^{-\Delta Ct}$. Data are represented as mean ± SEM. $^{*}p < 0.05$, $^{**}p < 0.01$, $^{***}p < 0.001$ when HA/βTCP compared to TPB, °p when compared to T0 and $^{\#}p$ when compared to 24 h. Two way ANOVA test was used for analysis of genes expression over time.

and higher expression level for h-OPN on HA/βTCP and for h-IBSP on TPB, confirm the impact of the scaffold on osteoblastic gene expression as seen *in vitro*. This differential expression may have an impact on bone formation as OPN has been shown to be an inhibitor of bone mineralization whereas IBSP promote it [45,46]. On the other hand, the other osteoblastic genes (Runx2 and OC) were preferentially expressed when hBMSC were grafted on TPB. Altogether, these results indicate that TPB favor hBMSC osteogenic potential, which may explain the faster bone formation obtained when TPB was used. The direct role of grafted hBMSC to form bone was then supported by the expression of human IBSP protein. Interestingly, immunostaining showed a chimeric bone with h-IBSP positive areas adjacent to a negative one. This result allowed us to confirm that host cells participate in new bone formation, as previously described [47]. Analysis of mouse osteoblastic genes including ALP, IBSP and OC showed that they were expressed only when hBMSC were seeded on biomaterials. These results indicated that hBMSC exert paracrine actions by stimulating chemoattraction and/or osteoblastic differentiation of host cells. Gene expression of chemokines described in the literature for their potential to recruit MSC (SDF-1, PDGFb, IGF1) was then analyzed. Neither SDF-1 nor PDGFb were expressed throughout the duration of the graft indicating that host MSC chemoattraction is not regulated by these pathways. In contrast, IGF1 was induced starting from 24 h and its expression increased over time. These results indicated that mouse MSC chemoattraction can be mediated by IGF1 secreted by grafted hBMSC and/or that IGF1 stimulates osteoblastic differentiation of host MSC [48] that were attracted by another chemokine as MCP-3 [49]. Taken together, our findings demonstrated the synergic direct and paracrine hBMSC roles [50] allowing the formation of chimeric bone.

Another crucial collaboration during bone regeneration is the osteoblastic/osteoclastic coupling. Bone resorption by osteoclasts is a critical step as it is the first phase of bone remodeling [38].

In our study, we showed that the graft of hBMSC enhance host osteoclastic activity as shown by TRAP positive staining and mRNA expression of mouse CTR and TRAP5b. Comparing both biomaterials we noticed that the first osteoclasts appeared at the same moment (2 W) but their number, functionality and the covered scaffold areas were higher on HA/βTCP. *In vitro* and *in vivo* analysis of human osteoclastogenic regulatory factor RANKL, showed that its mRNA expression was induced only when hBMSC were seeded on biomaterials. Interestingly, either *in vitro* or *in vivo* h-RANKL gene was more expressed when hBMSC were loaded on HA/βTCP. Whereas *in vitro* RANKL gene expression disappeared at 1 W, it continued to increase *in vivo* supporting the key role in both ways of "grafted cells/host cells" communication [50]. This communication may pass by inflammatory cells as we showed an up-regulation of m-Ly6C 24 h post-graft. In addition, hBMSC induced gene expression of host RANKL on HA/βTCP. Taken together, these results illustrate the primary role of grafted hBMSC on the control of host-derived osteoclastogenesis by paracrine effects to enhance osteoclastic activity [49,51]. Besides grafted cells, the associated scaffold can also play a role in this regulation. Higher osteoclastic activity induced by hBMSC on HA/βTCP can be explained by its massive granularity compared to TPB. Davison et al. demonstrated osteoclast sensitivity to scaffold architecture showing that small grain size promote osteoclastic differentiation [52]. Moreover, it has been shown that increasing the ratio of HA to 60% which is close to the composition of the used HA/βTCP scaffolds in our study, impair osteoblastic differentiation promoted by osteoclasts [53]. Taken together, these findings indicate that a higher osteoclastic activity on HA/βTCP impaired osteoclast/osteoblast balance. This can be explained by two mechanisms. (i) HA/βTCP orient hBMSC to promote osteoclastic activity preferentially than osteoblastic one, which disfavor bone formation. (ii) The increased osteoclastic activity on HA/βTCP may cause the concomitant resorption of neoformed bone decreasing the bone content on this scaffold. We know that the ideal bone substitute must be resorbable to be replaced by new bone in a fracture site [39]. However, an accelerated resorption results in bone loss as observed in postmenopausal osteoporosis, inflammatory arthritis or osteolytic bone metastasis [38]. Besides less hBMSC and their weaker osteogenic potential on HA/βTCP, our results indicate that a wide extent of osteoclastic activity, which imbalances osteoblast/osteoclast crosstalk, is another mechanism that disfavors bone formation on this biomaterial.

5. Conclusions

Our findings show that differences in bone formation depend on the biomaterial's capacity to select and guide MSC behavior. In bone tissue engineering, scaffolds provide a mechanical and biochemical microenvironment for MSC. The choice of the most appropriate biomaterial is crucial for a fast and complete bone repair. In this study, we have shown that collagen and smooth interconnected open porosity favor cell adhesion and migration, which improves bone formation. In contrast, a higher granularity promotes the osteoclastic activity induced by the grafted hBMSC, which disadvantages bone regeneration. The ongoing development of 3D bioprinting could allow the design of open structures similar to trabecular bone to facilitate the invasion, survival and *in vivo* engraftment of MSC as well as to control osteoclast activity in order to enhance bone formation.

Conflicts of interest

None.

Acknowledgments

This work was supported by EFS Ile de France (APR – 2014) and by the 7th Framework Program of the European Commission through the project REBORNE no. 241879. M. Mebarki was supported by Assistance Publique – Hôpitaux de Paris. The authors are grateful to Franck Chiappini for helpful statistical analysis, Guy Louarn from the Institut des Matériaux de Nantes, Béatrice Laurent and Sabine Louis for technical help, Najat Raddi for her critical review of the manuscript, Michael Marden for the rereading of the manuscript, SEM platform of University Paris-Est, with special thanks to Dr Patrick Ausset for his precious help and the Centre de Recherches Chirurgicales Dominique Chopin for animal platform facilities. The authors are grateful to the company Ceraver, which kindly provided the HA/βTCP ceramics.

References

[1] P.S. Lienemann, M.P. Lutolf, M. Ehrbar, Biomimetic hydrogels for controlled biomolecule delivery to augment bone regeneration, Adv. Drug Deliv. Rev. 64 (12) (2012) 1078–1089.
[2] T.J. Cypher, J.P. Grossman, Biological principles of bone graft healing, J. Foot Ankle Surg. Off. Publ. Am. Coll. Foot Ankle Surg. 35 (5) (1996) 413–417.
[3] T.A. Einhorn, L.C. Gerstenfeld, Fracture healing: mechanisms and interventions, Nat. Rev. Rheumatol. 11 (1) (2015) 45–54.
[4] Y. Homma, G. Zimmermann, P. Hernigou, Cellular therapies for the treatment of non-union: the past, present and future, Injury 44 (Suppl. 1) (2013) S46–49.
[5] C. Delloye, O. Cornu, V. Druez, O. Barbier, Bone allografts: what they can offer and what they cannot, J. Bone Joint Surg. Br. 89 (5) (2007) 574–579.
[6] B. Long, L. Dan, L. Jian, H. Yunyu, H. Shu, Y. Zhi, Evaluation of a novel reconstituted bone xenograft using processed bovine cancellous bone in combination with purified bovine bone morphogenetic protein, Xenotransplantation 19 (2) (2012) 122–132.
[7] V. Campana, G. Milano, E. Pagano, M. Barba, C. Cicione, G. Salonna, W. Lattanzi, G. Logroscino, Bone substitutes in orthopaedic surgery: from basic science to clinical practice, J. Mater. Sci. Mater. Med. 25 (10) (2014) 2445–2461.
[8] R.L. Deijkers, G.J. Bouma, E.M. van der Meer-Prins, P.E. Huysmans, A.H. Taminiau, F.H. Claas, Human bone allografts can induce T cells with high affinity for donor antigens, J. Bone Joint Surg. Br. 81 (3) (1999) 538–544.
[9] L. Coquelin, A. Fialaire-Legendre, S. Roux, A. Poignard, P. Bierling, P. Hernigou, N. Chevallier, H. Rouard, In vivo and in vitro comparison of three different allografts vitalized with human mesenchymal stromal cells, Tissue Eng. Part A 18 (2012) 1921–1931.
[10] V. Viateau, M. Manassero, L. Sensébé, A. Langonné, D. Marchat, D. Logeart-Avramoglou, H. Petite, M. Bensidhoum, Comparative study of the osteogenic ability of four different ceramic constructs in an ectopic large animal model, J. Tissue Eng. Regen. Med. 10 (3) (2016 Mar) E177–E187.
[11] H. Petite, V. Viateau, W. Bensaïd, A. Meunier, C. de Pollak, M. Bourguignon, K. Oudina, L. Sedel, G. Guillemin, Tissue-engineered bone regeneration, Nat. Biotechnol. 18 (9) (2000) 959–963.
[12] R. Cancedda, B. Dozin, P. Giannoni, R. Quarto, Tissue engineering and cell therapy of cartilage and bone, J. Int. Soc. Matrix Biol. 22 (1) (2003) 81–91.
[13] C. Chakar, N. Naaman, E. Soffer, N. Cohen, N. El Osta, H. Petite, F. Anagnostou, Bone formation with deproteinized bovine bone mineral or biphasic calcium phosphate in the presence of autologous platelet lysate: comparative investigation in rabbit, Int. J. Biomater. 2014 (2014) 367265.
[14] K.R. Garrison, I. Shemilt, S. Donell, J.J. Ryder, M. Mugford, I. Harvey, F. Song, V. Alt, Bone morphogenetic protein (BMP) for fracture healing in adults, Cochrane Database Syst. Rev. 6 (2010) 2–10 (CD006950).
[15] H. Kawaguchi, H. Oka, S. Jingushi, T. Izumi, M. Fukunaga, K. Sato, et al., A local application of recombinant human fibroblast growth factor 2 for tibial shaft fractures: a randomized, placebo-controlled trial, J. Bone Miner. Res. Off. J. Am. Soc. Bone Miner. Res. 25 (12) (2010) 2735–2743.
[16] M.F. Pittenger, A.M. Mackay, S.C. Beck, R.K. Jaiswal, R. Douglas, J.D. Mosca, M.A. Moorman, D.W. Simonetti, S. Craig, D.R. Marshak, Multilineage potential of adult human mesenchymal stem cells, Science 284 (5411) (1999) 143–147.
[17] S.A. Kuznetsov, M.H. Mankani, P.G. Robey, In vivo formation of bone and haematopoietic territories by transplanted human bone marrow stromal cells generated in medium with and without osteogenic supplements, J. Tissue Eng. Regen. Med. 7 (3) (2013) 226–235.
[18] M.H. Mankani, S.A. Kuznetsov, P.G. Robey, Formation of hematopoietic territories and bone by transplanted human bone marrow stromal cells requires a critical cell density, Exp. Hematol. 35 (6) (2007) 995–1004.
[19] A.L. Ponte, E. Marais, N. Gallay, A. Langonné, B. Delorme, O. Hérault, P. Charbord, J. Domenech, The in vitro migration capacity of human bone marrow mesenchymal stem cells: comparison of chemokine and growth factor chemotactic activities, Stem Cells Dayt. Ohio 25 (7) (2007) 1737–1745.
[20] T. Kitaori, H. Ito, E.M. Schwarz, R. Tsutsumi, H. Yoshitomi, S. Oishi, M. Nakano, N. Fujii, T. Nagasawa, T. Nakamura, Stromal cell-derived factor 1/CXCR4 signaling is critical for the recruitment of mesenchymal stem cells to the

fracture site during skeletal repair in a mouse model, Arthritis Rheum. 60 (3) (2009) 813–823.
[21] C.-Y. Lin, Y.-H. Chang, K.-J. Lin, T.-C. Yen, C.-L. Tai, C.-Y. Chen, W.-H. Lo, I.-T. Hsiao, Y.-C. Hu, The healing of critical-sized femoral segmental bone defects in rabbits using baculovirus-engineered mesenchymal stem cells, Biomaterials 31 (12) (2010) 3222–3230.
[22] M.B. Murphy, K. Moncivais, A.I. Caplan, Mesenchymal stem cells: environmentally responsive therapeutics for regenerative medicine, Exp. Mol. Med. 45 (2013) e54.
[23] A. Uccelli, L. Moretta, V. Pistoia, Mesenchymal stem cells in health and disease, Nat. Rev. Immunol. 8 (9) (2008) 726–736.
[24] L. Chen, E.E. Tredget, P.Y.G. Wu, Y. Wu, Paracrine factors of mesenchymal stem cells recruit macrophages and endothelial lineage cells and enhance wound healing, PLoS One 3 (4) (2008) e1886.
[25] A.-L. Gamblin, M.A. Brennan, A. Renaud, H. Yagita, F. Lézot, D. Heymann, V. Trichet, P. Layrolle, Bone tissue formation with human mesenchymal stem cells and biphasic calcium phosphate ceramics: the local implication of osteoclasts and macrophages, Biomaterials 35 (36) (2014) 9660–9667.
[26] R. Quarto, M. Mastrogiacomo, R. Cancedda, S.M. Kutepov, V. Mukhachev, A. Lavroukov, E. Kon, M. Marcacci, Repair of large bone defects with the use of autologous bone marrow stromal cells, N. Engl. J. Med. 344 (5) (2001) 385–386.
[27] C.J. Centeno, J.R. Schultz, M. Cheever, B. Robinson, M. Freeman, W. Marasco, Safety and complications reporting on the re-implantation of culture-expanded mesenchymal stem cells using autologous platelet lysate technique, Curr. Stem Cell Res. Ther. 5 (1) (2010) 81–93.
[28] M. Marcacci, E. Kon, V. Moukhachev, A. Lavroukov, S. Kutepov, R. Quarto, M. Mastrogiacomo, R. Cancedda, Stem cells associated with macroporous bioceramics for long bone repair: 6- to 7-year outcome of a pilot clinical study, Tissue Eng. 13 (5) (2007) 947–955.
[29] N. Chevallier, F. Anagnostou, S. Zilber, G. Bodivit, S. Maurin, A. Barrault, P. Bierling, P. Hernigou, P. Layrolle, H. Rouard, Osteoblastic differentiation of human mesenchymal stem cells with platelet lysate, Biomaterials 31 (2) (2010) 270–278.
[30] J. Leotot, L. Coquelin, G. Bodivit, P. Bierling, P. Hernigou, H. Rouard, N. Chevallier, Platelet lysate coating on scaffolds directly and indirectly enhances cell migration, improving bone and blood vessel formation, Acta Biomater. 9 (5) (2013) 6630–6640.
[31] C. Seebach, J. Schultheiss, K. Wilhelm, J. Frank, D. Henrich, Comparison of six bone-graft substitutes regarding to cell seeding efficiency, metabolism and growth behaviour of human mesenchymal stem cells (MSC) in vitro, Injury 41 (7) (2010) 731–738.
[32] F.J. O'Brien, B.A. Harley, I.V. Yannas, L.J. Gibson, The effect of pore size on cell adhesion in collagen-GAG scaffolds, Biomaterials 26 (4) (2005) 433–441.
[33] M.H. Mankani, S.A. Kuznetsov, B. Fowler, A. Kingman, P.G. Robey, In vivo bone formation by human bone marrow stromal cells: effect of carrier particle size and shape, Biotechnol. Bioeng. 72 (1) (2001) 96–107.
[34] J. Léotot, A. Lebouvier, P. Hernigou, P. Bierling, H. Rouard, N. Chevallier, Bone-forming capacity and biodistribution of bone marrow-derived stromal cells directly loaded into scaffolds: a novel and easy approach for clinical application of bone regeneration, Cell Transplant. 24 (10) (2015) 1945–1955.
[35] V.J. Cristofalo, R.G. Allen, R.J. Pignolo, B.G. Martin, J.C. Beck, Relationship between donor age and the replicative lifespan of human cells in culture: a reevaluation, Proc. Natl. Acad. Sci. U. S. A. 95 (18) (1998) 10614–10619.
[36] A. Lebouvier, A. Poignard, M. Cavet, J. Amiaud, J. Leotot, P. Hernigou, A. Rahmouni, P. Bierling, P. Layrolle, H. Rouard, N. Chevallier, Development of a simple procedure for the treatment of femoral head osteonecrosis with intra-osseous injection of bone marrow mesenchymal stromal cells: study of their biodistribution in the early time points after injection, Stem Cell Res. Ther. 6 (2015) 68.
[37] J. Gao, J.E. Dennis, R.F. Muzic, M. Lundberg, A.I. Caplan, The dynamic in vivo distribution of bone marrow-derived mesenchymal stem cells after infusion, Cells Tissues Organs 169 (1) (2001) 12–20.
[38] D.V. Novack, S.L. Teitelbaum, The osteoclast: friend or foe?, Annu Rev. Pathol. 3 (2008) 457–484.
[39] P. Bianco, P.G. Robey, Stem cells in tissue engineering, Nature 414 (6859) (2001) 118–121.
[40] A.P. Gilmore, Anoikis, Cell Death Differ. 12 (Suppl. 2) (2005) 1473–1477.
[41] F. Granero-Moltó, T.J. Myers, J.A. Weis, L. Longobardi, T. Li, Y. Yan, N. Case, J. Rubin, A. Spagnoli, Mesenchymal stem cells expressing insulin-like growth factor-I (MSCIGF) promote fracture healing and restore new bone formation in Irs1 knockout mice: analyses of MSCIGF autocrine and paracrine regenerative effects, Stem Cells Dayt. Ohio 29 (10) (2011) 1537–1548.
[42] K.L. Yao, R. Todescan, J. Sodek, Temporal changes in matrix protein synthesis and mRNA expression during mineralized tissue formation by adult rat bone marrow cells in culture, J. Bone Miner. Res. Off. J. Am. Soc. Bone Miner. Res. 9 (2) (1994) 231–240.
[43] J. Chen, M.D. McKee, A. Nanci, J. Sodek, Bone sialoprotein mRNA expression and ultrastructural localization in fetal porcine calvarial bone: comparisons with osteopontin, Histochem. J. 26 (1) (1994) 67–78.
[44] R. McBeath, D.M. Pirone, C.M. Nelson, K. Bhadriraju, C.S. Chen, Cell shape, cytoskeletal tension, and RhoA regulate stem cell lineage commitment, Dev. Cell 6 (4) (2004) 483–495.
[45] J.R. de Bruyn, M. Goiko, M. Mozaffari, D. Bator, R.L. Dauphinee, Y. Liao, R.L. Flemming, M.S. Bramble, G.K. Hunter, H.A. Goldberg, Dynamic light scattering study of inhibition of nucleation and growth of hydroxyapatite crystals by osteopontin, PLoS One 8 (2) (2013) e56764. doi: 10.1371R.
[46] E. Holm, J.E. Aubin, G.K. Hunter, F. Beier, H.A. Goldberg, Loss of bone sialoprotein leads to impaired endochondral bone development and mineralization, Bone 71 (2015) 145–154. doi: 10.1016.
[47] R. Tasso, F. Fais, D. Reverberi, F. Tortelli, R. Cancedda, The recruitment of two consecutive and different waves of host stem/progenitor cells during the development of tissue-engineered bone in a murine model, Biomaterials 31 (8) (2010) 2121–2129.
[48] L. Xian, X. Wu, L. Pang, M. Lou, C.J. Rosen, T. Qiu, J. Crane, F. Frassica, L. Zhang, J. P. Rodriguez, Xiaofeng Jia, Shoshana Yakar, Shouhong Xuan, Argiris Efstratiadis, Mei Wan, Xu Cao, Matrix IGF-1 maintains bone mass by activation of mTOR in mesenchymal stem cells, Nat. Med. 18 (7) (2012) 1095–1101.
[49] K. Shinohara, S. Greenfield, H. Pan, A. Vasanji, K. Kumagai, R.J. Midura, M. Kiedrowski, M.S. Penn, G.F. Muschler, Stromal cell-derived factor-1 and monocyte chemotactic protein-3 improve recruitment of osteogenic cells into sites of musculoskeletal repair, J. Orthop. Res. Off. Publ. Orthop. Res. Soc. 29 (7) (2011) 1064–1069.
[50] M.Á. Brennan, A. Renaud, J. Amiaud, M.T. Rojewski, H. Schrezenmeier, D. Heymann, V. Trichet, P. Layrolle, Pre-clinical studies of bone regeneration with human bone marrow stromal cells and biphasic calcium phosphate, Stem Cell Res. Ther. 5 (5) (2014) 114.
[51] R. Tasso, V. Ulivi, D. Reverberi, C. Lo Sicco, F. Descalzi, R. Cancedda, In vivo implanted bone marrow-derived mesenchymal stem cells trigger a cascade of cellular events leading to the formation of an ectopic bone regenerative niche, Stem Cells Dev. 22 (24) (2013) 3178–3191.
[52] N.L. Davison, B. ten Harkel, T. Schoenmaker, X. Luo, H. Yuan, V. Everts, F. Barrère-de Groot, J.D. de Bruijn, Osteoclast resorption of beta-tricalcium phosphate controlled by surface architecture, Biomaterials 35 (26) (2014) 7441–7451.
[53] Y. Shiwaku, L. Neff, K. Nagano, K.-I. Takeyama, J. de Bruijn, M. Dard, F. Gori, R. Baron, The crosstalk between osteoclasts and osteoblasts is dependent upon the composition and structure of biphasic calcium phosphates, PLoS One 10 (7) (2015) e0132903.